

# Optical satellite tracking in Earth's shadow with non-traditional illumination

**Kevin Schafer**

*MITRE Corporation, 1155 Academy Park Loop, Colorado Springs, CO 80910*

**David Marson**

*MITRE Corporation, 202 Burlington Road, Bedford, MA 01730*

## ABSTRACT

Passive optical tracking of satellites relies on sunlight reflecting from satellites for target illumination. However, when satellites enter Earth's shadow, brightness of the target dramatically decreases. Unless active tracking methods are employed, such as radar or laser systems, the target track is lost. Active tracking systems are expensive and limited in number, making them difficult to access or acquire. They also generate a signal or signature that can be detected by the target or other sensors, giving away the active tracking system's intentions.

The night side of Earth does emit light, much of it from artificial sources concentrated in population centers or cities. Previous efforts have observed the possibility of using this artificial light, or "city shine," as a source of illumination for satellites in Earth's shadow. This work explores and quantifies leveraging city shine to track satellites in Earth's shadow using ground-based optical sensors, thereby increasing space domain awareness capabilities with cost-effective passive systems.

## 1. INTRODUCTION

Traditionally, the best times for Low Earth Orbit (LEO) optical tracking are shortly after sunset and shortly before sunrise, when the sun is out of sight of an Earth-based observer but visible to and can be reflected off satellites orbiting overhead. However, when satellites are partially shadowed in penumbra or completely shadowed in umbra, the intensity of light reflecting off satellites decreases or disappears. When reflected sunlight is not viable, a possible source of illumination is Earth's nighttime light emissions.

These emissions largely come from the artificial lights in cities, called "city shine." City shine is an attractive source for nighttime target illumination because of its reliable and ever present magnitude. In fact, Earth's total artificially lit outdoor area and total radiance have been continuously growing [1]. Combined with the availability and relatively low cost of optical sensors, an opportunity exists to increase satellite tracking coverage through inexpensive means.

## 2. IMPACT ANALYSIS

To verify potential utility of city shine as a satellite illuminator, modeling and simulation tools were utilized to identify the number of medium to large\* [2] LEO satellites in Earth's shadow whose orbits intersected the fields of view (FOV) of randomly selected major metropolitan areas during a 12-hour period. Many satellites were identified to traverse from sunlit to Earth's shadow, which represents opportunities to track a satellite beyond current sunlit-dependent techniques.

Fig. 1 shows a sensor's 12-hour coverage opportunities for tracking satellites that traverse from sunlit condition into Earth shadow or cross sensor FOV completely in Earth shadow. Each interval on the histogram shown in Fig. 1 contains the amount of possible tracking on satellites in sensor coverage for a given interval. For example, from 02:35 – 03:11 (one interval = 36 minutes), over 500 minutes of tracks are possible on 181 unique satellites. This analysis quantifies amount of tracking on satellites cumulatively, yet only counts a unique satellite once if tracked multiple times during the 12-hour window. As expected, more satellites are sunlit detectable at the beginning and end of the 12-hour window, and more satellites cross Earth shadow in the middle of the 12-hour window.

\*Medium (0.1m<sup>2</sup> – 1m<sup>2</sup>), Large (>1m<sup>2</sup>) [2]

**Approved for Public Release; Distribution Unlimited. Public Release Case Number 21-2545**

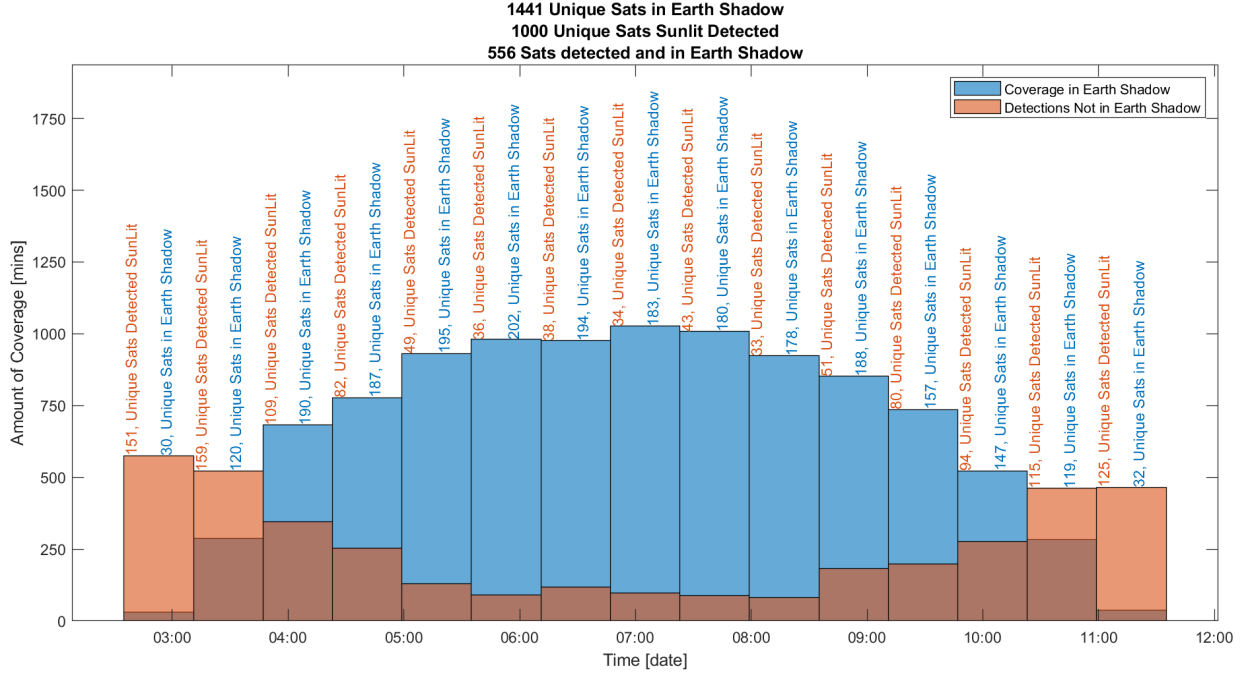


Fig 1. Single sensor FOV coverage

### 3. MODELING AND SIMULATION

After analyzing potential impact, a simplified model of the physics behind the city shine concept was developed. The simulation calculates the amount of light from an emitter on the ground that reflects off a satellite directly overhead and is received by a ground-based optical sensor. The emitter, satellite, and sensor properties were parameterized for concept exploration of over 21,000 simulated combinations. A signal-to-noise (SNR) metric was generated based on the amount of light that reaches the optical sensor versus background sky brightness. Results showed that many combinations were able to achieve an SNR greater than or equal to two. For a meter-class telescope, medium satellites were simulated to surpass this SNR threshold at altitudes greater than 500 km, and large satellites were calculated to be detectable at altitudes greater than 1000 km.

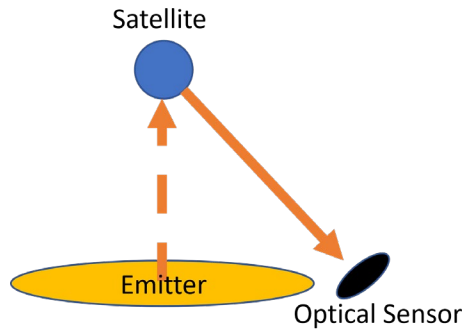


Fig. 2. Simple radiance estimate

Consider radiative exchange between two finite areas, emitter and satellite, as depicted in Fig. 2. The fraction of energy leaving the emitter that arrives at the satellite is expressed as [3]:

$$F_{1 \rightarrow 2} = \frac{1}{A_1} \int_{A_1} \int_{A_2} \frac{\cos \beta_1 \cos \beta_2}{\pi S^2} dA_1 dA_2 \quad (1)$$

Where  $A_1$  is area of emitter,  $A_2$  is area of satellite,  $\beta_1$  is angle from emitter normal to satellite,  $\beta_2$  is angle from satellite normal to emitter, and  $S$  is range between emitter and satellite. For the simple radiance estimate used in this work, emitter is assumed to be flat and the satellite is modeled as a sphere directly overhead. Radiant power ( $R_e$ ) in watts at the satellite is expressed as:

$$R_e = I \frac{1}{S^2} A_1 A_2 \quad (2)$$

where  $I$  is intensity in watts per area steradian. Using the same assumptions from (2), with respect to radiant power reflected by spherical satellite ( $R_s$ ) in watts per steradian results in:

$$R_s = \frac{R_e}{2\pi} \quad (3)$$

Note that  $2\pi$  steradian is used in the denominator of (3) since it is assumed that there is half-sphere reflectance as shown in Fig. 2. Optical sensor is at some offset angle. This is an important concept of city shine satellite illumination, since it is unlikely that an optical sensor collocated with an emitter could detect a satellite in the presence of overwhelming background scatter. Radiant power that reaches the optical sensor ( $R_o$ ) in watts is expressed as:

$$R_o = R_s \frac{\cos \beta_1 \cos \beta_2}{r^2} A_t \quad (4)$$

where  $r$  is the range between satellite and optical sensor and  $A_t$  is the aperture area of the telescope component of the optical sensor.

$R_o$  is used as an input for computing SNR, which ultimately is used to infer satellite detection. User-selectable parameters are shown in Table 1.

Table 1. User parameters

Component	Parameter(s)
Night sky	Sky background magnitude Sky transmission
Emitter	Mean radiance (simplified estimate) Diameter (simplified estimate) Radiance bandwidth
Satellite	Optical cross-sectional area Location Albedo
Telescope	Aperture diameter Field stop number Optic transmission Location Filter center wavelength Filter spectral bandwidth
Camera	Pixel side lengths Quantum efficiency Integration time Dark current

The optical sensor model is based on light,  $R_o$ , passing through a telescope and being sensed by a digital camera (CCD, sCMOS, etc.).  $R_o$  and sky background are refined by several telescope parameters, including aperture diameter, field stop number, optic transmission, filter center wavelength, and filter spectral bandwidth. The resulting light signal is distributed across simulated center pixels, and sky background is applied in a pseudo-random fashion to each pixel, contributing to simulated background noise on the detector. The camera model parameters include pixel size, quantum efficiency, integration time, and dark current. An example resulting model is shown in Fig. 3.

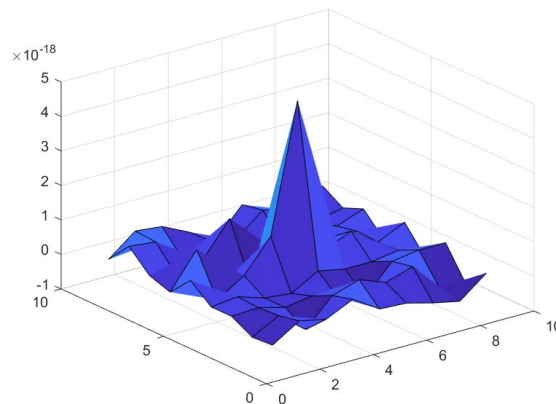


Fig. 3. Simulated detector response

A classic aperture photometry technique, consisting of concentric circles centered around the strongest signal, is employed (Fig. 4). Expecting weak signals when dealing with city shine-lit satellites, an SNR of 2 was chosen as the detection threshold. Fig. 10(b) shows an example of a low SNR around 2 as detectable.

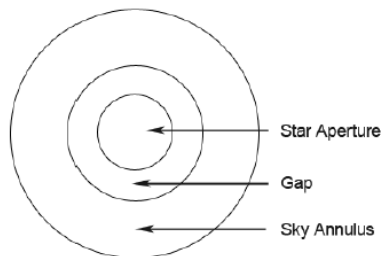


Fig. 4. Aperture photometry diagram [4]

To further enhance the simulation's fidelity, a day-night band (DNB) global nighttime radiance data set generated by the National Aeronautics and Space Administration (NASA)/National Oceanographic and Atmospheric Administration (NOAA) Visible Infrared Imaging Radiometer Suite (VIIRS) project [5] was incorporated, creating a more detailed calculation method. The data are presented in a 15 arc-second geographic grid that contains over 55 million nighttime radiance measurements.

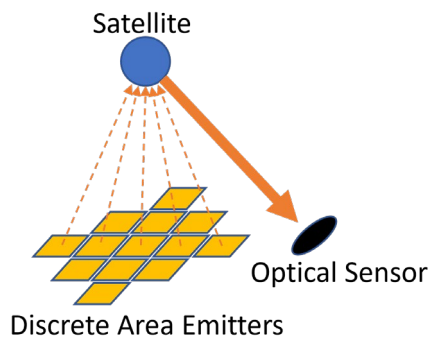


Fig. 5. Detailed radiance estimate

Fig. 5 illustrates the detailed method employed that incorporates VIIRS radiance at discrete areas on Earth’s surface. By developing satellite FOV calculations, the model was expanded to allow more flexible satellite position definitions and include real light source measurements in emitter calculations.

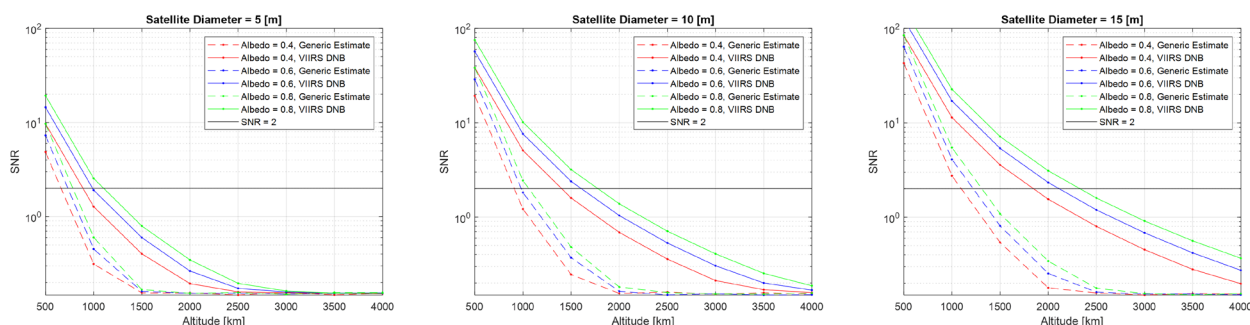


Fig. 6. Altitude vs. SNR large satellite; simple and detailed

Fig. 6 shows SNR versus altitude with a selected set of parameters, listed in Table 2, for comparison between the simplified (generic, treating the emitter as a single area) and detailed (incorporating VIIRS radiance data) SNR estimates. This series of exploratory simulations showed that simplified model assumptions were underestimating the amount of city shine reaching the satellite. This scenario with user-selected parameters shows a realizable optical sensor’s potential utility tracking satellites with city shine illumination. Fig. 6 shows that a spherical satellite of 5-meter diameter is detectable from 500 to 1000 km. As satellite size and albedo increase, detectability increases for higher altitudes.

Table 2. Fixed user-selected parameters

Parameter	Value
Telescope aperture diameter	1 m
Telescope field stop number	6
Telescope optic transmission	0.9
Telescope filter spectral bandwidth	80 nm
Telescope filter center wavelength	500 nm
Camera integration time	60 seconds
Camera pixel side lengths	6.50 x 10 <sup>-6</sup> m
Camera quantum efficiency	0.82
Emitter diameter (simple case)	100 km

Emitter mean radiance (simple case)	17 nW cm <sup>-2</sup> sr <sup>-1</sup>
Night sky background magnitude	21.69
Night sky transmission	0.7

#### 4. EXPERIMENTATION

The catalyst for this work was an ad hoc observation attempt of the International Space Station (ISS) as it passed over Tokyo, Japan. A portable optical sensor site was set up in Nagano, Japan, located approximately 180 km from Tokyo. Equipment on hand was a Takahashi FSQ-106ED, an Andor Zyla 4.2+, and a Paramount MyT, seen in Fig. 7. The latest ISS two line element set (TLE) from space-track.org was propagated, and resulting positions were used to point the Paramount MyT at the ISS while it crossed overhead in Earth shadow. Fig. 8 shows the propagated path used to drive the telescope mount. A camera exposure time of 3.5 seconds was used, while camera coolers were set to 0° C. Additionally, a hardware trigger was used to start camera exposure, with the trigger source being a transistor transistor logic pulse per second from a Global Positioning System time signal-disciplined computer clock. After exposure start, the camera’s internal timekeeping mechanism set the exposure duration. Eight images of the ISS detected by suspected (at time of collection) city shine illumination were captured. An example is shown on Fig. 10(a). The images are separated by five seconds between start times.

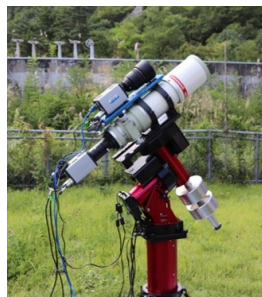


Fig. 7. Equipment used in Nagano, Japan



Fig. 8. TLE-propagated ISS positions

This scenario was recreated with the modeling and simulation capability by incorporating accurate telescope and camera parameters, VIIRS data, and the same TLE-propagated satellite positions originally used to drive the telescope mount in Nagano, Japan. Simulation results found that, with best case assumptions for the station’s cross-sectional area and albedo, detections achieve an SNR of nearly 1.8, shown in Fig. 9.

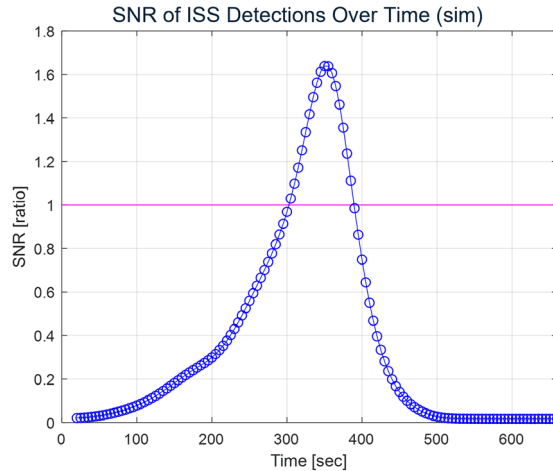


Fig. 9. Modeling and simulation SNR vs. time; ISS pass over Japan

This result matches well with raw experiment data showing an SNR of 2.7 seen in Fig. 10(b). These results warrant further study into the feasibility of the city shine technique for satellite detection.

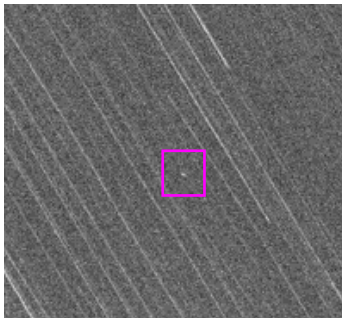


Fig. 10(a). Raw data from experiment collection

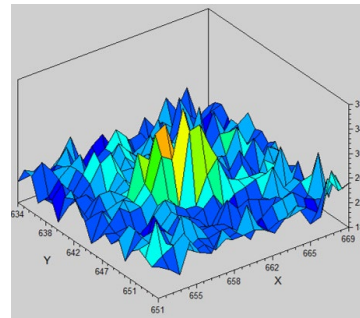


Fig. 10(b). Collection SNR = 2.7

## 5. SUMMARY AND FUTURE WORK

This work built a modeling and simulation capability for determining SNR of city shine-illuminated satellites. Several camera and telescope parameters were included, thereby successively increasing the fidelity of the model. A simple estimate modeling and simulation capability is the foundation of this work. By incorporating VIIRS data, satellite positions, and optical sensor locations, a detailed modeling and simulation capability resulted. The simplified model retains agnostic properties and is adaptable to other data sets and is prime for capability expansion. The detailed model as an extension of the simplified model shows utility as a predictor of optical sensors' abilities to detect city shine-illuminated satellites. One experimental data set was used for comparison of real-world optical sensor performance tracking city shine-illuminated satellites in Earth shadow. Future work is planned encompassing more detailed modeling and simulation and collecting more real-world experiment data. Also of note is Fig. 11, showing emission spectrums of typical streetlamps, which contribute greatly to city shine. The VIIRS DNB relative spectral response, [6] as seen in Fig. 11, has bandwidth from  $\approx 500\text{--}900\text{ nm}$ , which does not capture a large portion of light-emitting diode (LED) emissions. These emissions contribute to a city shine-lit satellite signal; most silicon-based detectors respond to this bandwidth. VIIRS data used in this work does not completely capture city shine radiance by not including LED contributions in the  $400\text{--}500\text{ nm}$  bandwidth. Future work also includes exploring incorporating the  $400\text{--}500\text{ nm}$  bandwidth LED contributions.

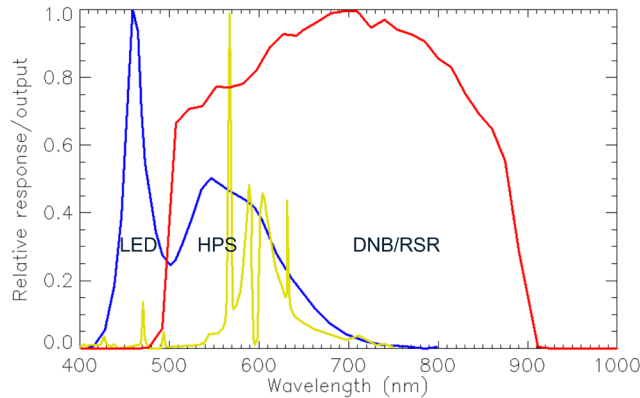


Fig. 11. Typical LED and high-pressure sodium lamp spectrums [6]

## 6. ACKNOWLEDGEMENTS

The authors would like to acknowledge Dr. Ariel Schlamm, whose mentorship and guidance made this work possible. The authors would also like to extend special thanks to Robert Nolan for technical contributions that were pivotal for modeling and simulation used in this work.

## 7. REFERENCES

- [1] C. C. M. Kyba, T. Kuester, A. Sánchez de Miguel, K. Baugh, A. Jechow, F. Hölker, J. Bennie, C. D. Elvidge, K. J. Gaston and L. Guanter, "Artificially lit surface of Earth at night increasing in radiance and extent," *Science Advances*, vol. 3, no. 11, p. e1701528, 2007.
- [2] "space-track.org," CFSCC CJ3/6, [Online]. Available: <https://www.space-track.org/documentation#faq>. [Accessed 01 August 2021].
- [3] J. R. Howell and R. Siegel, "Thermal Radiation Heat Transfer. II - Radiation Exchange Between Surfaces and in Enclosures," Scientific and Technical Information Division NASA SP-164, Cleveland, Ohio, 1969.
- [4] The American Association of Variable Star Observers, "The AAVSO Guide to CCD Photometry," Cambridge, MA, 2014.
- [5] "Visible Infrared Imaging Radiometer Suite (VIIRS) | Earthdata," NASA/NOAA, [Online]. Available: <https://earthdata.nasa.gov/earth-observation-data/near-real-time/download-nrt-data/viirs-nrt>.
- [6] C. Cao and Y. Bai, "Quantitative Analysis of VIIRS DNB Nightlight Point Source for Light Power Estimation and Stability Monitoring," *Remote Sensing*, vol. 6, no. 12, pp. 11915-11935, 2014.